Electronic structure and orbital ordering in perovskite-type 3*d* transition-metal oxides studied by Hartree-Fock band-structure calculations

T. Mizokawa and A. Fujimori
Department of Physics, University of Tokyo, Bunkyo-ku, Tokyo 113, Japan
(Received 5 February 1996)

We have studied transition-metal 3*d*-oxygen 2*p* lattice models, where full degeneracy of transition-metal 3*d* and oxygen 2*p* orbitals and on-site Coulomb and exchange interactions between 3*d* electrons are taken into account, by means of a spin- and orbital-unrestricted Hartree-Fock (HF) approximation. The electronic-structure parameters deduced from the cluster-model analyses of the photoemission spectra are used as input. We have applied this method to perovskite-type 3*d* transition-metal oxides, which exhibit various electrical and magnetic properties. It is shown that the HF results can explain the ground-state properties of insulating oxides. The relationship between spin- and orbital-ordered solutions and the Jahn-Teller-type and $GdFeO_3$-type distortions in $RTiO_3$, RVO_3, $RMnO_3$, and $RNiO_3$ (R is a rare earth atom or Y) is extensively studied. Single-particle excitation spectra calculated using Koopmans' theorem give us an approximate but relevant picture on the electronic structure of the perovskite-type 3*d* transition-metal oxides. As a drawback, the HF calculations tend to overestimate the magnitude of the band gap compared with the experimental results and to predict some paramagnetic metals as antiferromagnetic insulators. [S0163-1829(96)03432-7]

I. INTRODUCTION

In recent decades, there have been many attempts to understand a variety of electrical and magnetic properties of 3*d* transition-metal oxides, especially their metal-insulator transitions.[1] Mott and Hubbard have shown that the strong *d*-*d* Coulomb interaction is essential to explain why many 3*d* transition-metal compounds with a partially filled 3*d* band can exist as magnetic insulators:[2,3] When the width of the 3*d* band is larger than the *d*-*d* Coulomb interaction, the compound becomes metallic. When the *d*-*d* Coulomb interaction exceeds the bandwidth, the 3*d* electrons are localized and the compound turns into an insulator with local magnetic moment, the band gap of which is determined by the magnitude of the *d*-*d* Coulomb interaction. The essential point of the Mott-Hubbard-type metal-insulator transition is described by the single-band Hubbard model.[3] However, in real compounds, the degeneracy of the 3*d* orbitals makes the symmetry-broken state of the magnetic insulator complicated and might affect the metal-insulator transition. In order to study the effect of the orbital degeneracy in the insulating state, a degenerate-band Hubbard model has been studied by applying an unrestricted Hartree-Fock (HF) approximation to the Coulomb-interaction term and by constructing an effective Hamiltonian through second-order perturbation with respect to the hybridization term.[4–8] Castellani, Natoli, and Ranninger have applied the unrestricted HF calculation to a realistic degenerate Hubbard model for V_2O_3, where the hopping term reflects the corrundum structure.[7] Ashkenazi and Weger have also studied the metal-insulator transitions of Ti_2O_3 and V_2O_3 using the HF method.[8] The validity of the unrestricted HF approach to the Mott insulators has generally been discussed by Brandow.[9] However, in those calculations, the O 2*p* orbitals were not explicitly included and the only transfer integrals between effective *d* orbitals, which correspond to the antibonding band formed by the hybridization between the transition-metal 3*d* and oxygen 2*p* orbitals, were considered.

Following the development of photoemission spectroscopy, Fujimori and Minami have shown that the band gap of NiO is not determined by *d*-*d* Coulomb interaction, but by oxygen-to-metal 3*d* charge-transfer energy from the NiO_6 cluster-model calculation.[10] Zaanen, Sawatzky, and Allen and Hüfner have provided a clear classification scheme, a so-called Zaanen-Sawatzky-Allen scheme, based on the Anderson-impurity model,[11] in which transition-metal compounds can be classified into two regimes according to the relative magnitudes of the ligand-to-metal charge-transfer energy Δ and *d*-*d* Coulomb energy U. In the Mott-Hubbard regime, where $\Delta > U$, the band gap corresponds to charge fluctuations of the *d*-*d* type, $d^n + d^n \rightarrow d^{n+1} + d^{n-1}$ and its magnitude is essentially given by $\sim U$. In the charge-transfer regime, where $\Delta < U$, charge fluctuations of the type $d^n + d^n \rightarrow d^{n+1} + d^n\underline{L}$ constitute a *p*-*d*-type band gap, the magnitude of which is $\sim \Delta$. Therefore, in order to investigate the metal-insulator transition in which the charge-transfer-type band-gap collapses, it is essential to explicitly include the ligand *p* orbitals in the model. On the other hand, the cluster and Anderson-impurity models, which have succeeded in reproducing the photoemission spectra and extracting the important electronic-structure parameters Δ and U, neglect the translational symmetry of the crystals. Furthermore, there has been ample experimental and theoretical evidence that magnetic ordering and lattice distortion strongly influences metal-insulator transitions in the 3*d* transition-metal oxides. Therefore, it is difficult to study the metal-insulator transition by using the cluster and Anderson-impurity models.

Recently, we have studied transition-metal 3*d*-oxygen 2*p* lattice models, where full degeneracy of transition-metal 3*d* and oxygen 2*p* orbitals and on-site Coulomb and exchange interactions for transition-metal sites are taken into

 © 1996 The American Physical Society

account, by means of spin- and orbital-unrestricted Hartree-Fock (HF) approximations in order to refine the previous HF method[6–8] by including oxygen $2p$ orbitals explicitly and to extend the cluster-model calculation by including the translational symmetry of the $3d$ orbitals.[12] We have shown that this method is powerful to study magnetic and orbital ordering and the effect of lattice distortion on it and the band gaps, and applied the method to $R\mathrm{TiO_3}$ (R=rare earth or Y), $R\mathrm{MnO_3}$, and $R\mathrm{NiO_3}$. On the other hand, there have been some attempts to study the orbital ordering in $3d$ transition-metal compounds using *ab initio* band-structure calculation. It has been shown that *ab initio* HF calculation can correctly predict the orbital ordering in $\mathrm{KCuF_3}$.[13] The LDA+U method, in which the energy functional is that of the local-density approximation plus parametrized HF terms as an approximation to the on-site Coulomb interaction term,[14] has also been applied to $\mathrm{KCuF_3}$ successfully.[15] Since these *ab initio* calculations require relatively much computational time, it is hard to study many compounds in a systematic manner. In this paper, we have systematically applied the model HF calculation to a large amount of perovskite-type $3d$ transition-metal oxides, $\mathrm{RMO_3}$ (M=Ti, V, Cr, Mn, Fe, Co, Ni, Cu). The organization of this paper is as follows. In Sec. II, we explain how to apply the unrestricted HF approximation to the perovskite-type lattice model. In Sec. III, results of the HF calculation for the various perovskite-type $3d$ transition-metal oxides are presented. Finally, we summarize the results of the unrestricted HF calculations and discuss the limitation of the HF approximation in Sec. IV.

II. UNRESTRICTED HARTREE-FOCK APPROXIMATION

We have applied the unrestricted HF approximation to the multiband d-p model, where tenfold degeneracy of the transition-metal $3d$ orbitals and sixfold degeneracy of the oxygen $2p$ orbitals are taken into account. The interatomic $3d$-$3d$ Coulomb interaction is expressed by Kanamori parameters, u, u', j, and j'.[16] We have to assume the relationship $u'=u-2j$ and $j'=j$ in order to keep the rotational invariance in real space of the Coulomb terms.[9,16] The Hamiltonian is given by

$$H=H_d+\varepsilon_p\sum_{k,l,\sigma}p^\dagger_{\mathbf{k},l\sigma}p_{\mathbf{k},l\sigma}+\sum_{\mathbf{k},l>l',\sigma}V^{pp}_{\mathbf{k},ll'}p^\dagger_{\mathbf{k},l\sigma}p_{\mathbf{k},l'\sigma}+\text{H.c.}+\sum_{\mathbf{k},l,\beta m,\sigma}V^{pd}_{\mathbf{k},l\beta m}p^\dagger_{\mathbf{k},l\sigma}d_{\mathbf{k},\beta m\sigma}+\text{H.c.}, \tag{1}$$

$$\begin{aligned}H_d=&\varepsilon^0_d\sum_{\alpha,\beta,m,\sigma}d^\dagger_{\alpha,\beta m\sigma}d_{\alpha,\beta m\sigma}+\sum_{\alpha,\beta,m,m',\sigma,\sigma'}h_{m\sigma,m'\sigma'}d^\dagger_{\alpha,\beta m\sigma}d_{\alpha,\beta m'\sigma'}+\sum_{\alpha,\beta,m}ud^\dagger_{\alpha,\beta m\uparrow}d_{\alpha,\beta m\uparrow}d^\dagger_{\alpha,\beta m\downarrow}d_{\alpha,\beta m\downarrow}\\&+\sum_{\alpha,\beta,m\neq m'}u'd^\dagger_{\alpha,\beta m\uparrow}d_{\alpha,\beta m\uparrow}d^\dagger_{\alpha,\beta m'\downarrow}d_{\alpha,\beta m'\downarrow}+\sum_{\alpha,\beta,m>m',\sigma}(u'-j)d^\dagger_{\alpha,\beta m\sigma}d_{\alpha,\beta m\sigma}d^\dagger_{\alpha,\beta m'\sigma}d_{\alpha,\beta m'\sigma}\\&+\sum_{\alpha,\beta,m\neq m'}j'd^\dagger_{\alpha,\beta m\uparrow}d_{\alpha,\beta m'\uparrow}d^\dagger_{\alpha,\beta m\downarrow}d_{\alpha,\beta m'\downarrow}+\sum_{\alpha,\beta,m\neq m'}jd^\dagger_{\alpha,\beta m\uparrow}d_{\alpha,\beta m'\uparrow}d^\dagger_{\alpha,\beta m'\downarrow}d_{\alpha,\beta m\downarrow},\end{aligned} \tag{2}$$

where $d^\dagger_{\mathbf{k},\beta m\sigma}\equiv(1/\sqrt{N})\Sigma_\alpha e^{i\mathbf{k}\cdot\mathbf{R}_\alpha}d^\dagger_{\alpha,\beta m\sigma}$ and $p^\dagger_{\mathbf{k},l\sigma}$ are creation operators for Bolch electrons constructed from the transition-metal $3d$ and oxygen $2p$ orbitals, respectively. α and $\mathbf{k}$ label the unit cell and the wave vector in the first Brillouin zone. β and m are indices for the transition-metal atoms in the unit cell and the $3d$ orbitals on the transition-metal atom, respectively. l denotes the $2p$ orbitals in the unit cell. $V^{pp}_{\mathbf{k},ll'}$ and $V^{pd}_{\mathbf{k},lm}$ are $2p$-$2p$ and $2p$-$3d$ transfer integrals. $h_{m\sigma,m'\sigma'}$ represents the crystal field and spin-orbit interaction of the $3d$ orbitals. Using the unrestricted HF approximation, the mean-field Hamiltonian becomes

$$H^{\mathrm{MF}}_d=\varepsilon^0_d\sum_{\alpha,\beta,m\sigma}d^\dagger_{\alpha,\beta m\sigma}d_{\alpha,\beta m\sigma}+\sum_{\alpha,\beta,m\sigma,m'\sigma'}h_{m\sigma,m'\sigma'}d^\dagger_{\alpha,\beta m\sigma}d_{\alpha,\beta m'\sigma'}+\sum_{\alpha,\beta,m}u\langle d^\dagger_{\alpha,\beta m\uparrow}d_{\alpha,\beta m\uparrow}\rangle d^\dagger_{\alpha,\beta m\downarrow}d_{\alpha,\beta m\downarrow} \tag{3}$$

$$\begin{aligned}&+\sum_{\alpha,\beta,m}ud^\dagger_{\alpha,\beta m\uparrow}d_{\alpha,\beta m\uparrow}\langle d^\dagger_{\alpha,\beta m\downarrow}d_{\alpha,\beta m\downarrow}\rangle-\sum_{\alpha,\beta,m}u\langle d^\dagger_{\alpha,\beta m\uparrow}d_{\alpha,\beta m\uparrow}\rangle\langle d^\dagger_{\alpha,\beta m\downarrow}d_{\alpha,\beta m\downarrow}\rangle\\&+\sum_{\alpha,\beta,m\neq m'}u'\langle d^\dagger_{\alpha,\beta m\uparrow}d_{\alpha,\beta m\uparrow}\rangle d^\dagger_{\alpha,\beta m'\downarrow}d_{\alpha,\beta m'\downarrow}+\sum_{\alpha,\beta,m\neq m'}u'd^\dagger_{\alpha,\beta m\uparrow}d_{\alpha,\beta m\uparrow}\langle d^\dagger_{\alpha,\beta m'\downarrow}d_{\alpha,\beta m'\downarrow}\rangle\\&-\sum_{\alpha,\beta,m\neq m'}u'\langle d^\dagger_{\alpha,\beta m\uparrow}d_{\alpha,\beta m\uparrow}\rangle\langle d_{\alpha,\beta m'\downarrow}d_{\alpha,\beta m'\downarrow}\rangle+\sum_{\alpha,\beta,m>m',\sigma}(u'-j)\langle d^\dagger_{\alpha,\beta m\sigma}d_{\alpha,\beta m\sigma}\rangle d^\dagger_{\alpha,\beta m'\sigma}d_{\alpha,\beta m'\sigma}\\&+\sum_{\alpha,\beta,m>m',\sigma}(u'-j)d^\dagger_{\alpha,\beta m\sigma}d_{\alpha,\beta m\sigma}\langle d^\dagger_{\alpha,\beta m'\sigma}d_{\alpha,\beta m'\sigma}\rangle-\sum_{\alpha,\beta,m>m',\sigma}(u'-j)\langle d^\dagger_{\alpha,\beta m\sigma}d_{\alpha,\beta m\sigma}\rangle\langle d^\dagger_{\alpha,\beta m'\sigma}d_{\alpha,\beta m'\sigma}\rangle\\&-\sum_{\alpha,\beta,m>m',\sigma}(u'-j)\langle d_{\alpha,\beta m\sigma}d_{\alpha,\beta m'\sigma}\rangle d^\dagger_{\alpha,\beta m'\sigma}d_{\alpha,\beta m\sigma}-\sum_{\alpha,\beta,m>m',\sigma}(u'-j)d^\dagger_{\alpha,\beta m\sigma}d_{\alpha,\beta m'\sigma}\langle d^\dagger_{\alpha,\beta m'\sigma}d_{\alpha,\beta m\sigma}\rangle\end{aligned}$$

$$+\sum_{\alpha,\beta,m>m',\sigma}(u'-j)\langle d^{\dagger}_{\alpha,\beta m\sigma}d_{\alpha,\beta m'\sigma}\rangle\langle d^{\dagger}_{\alpha,\beta m'\sigma}d_{\alpha,\beta m\sigma}\rangle+\sum_{\alpha,\beta,m\neq m'}j'\langle d^{\dagger}_{\alpha,\beta m\uparrow}d_{\alpha,\beta m'\uparrow}\rangle d^{\dagger}_{\alpha,\beta m\downarrow}d_{\alpha,\beta m'\downarrow}$$

$$+\sum_{\alpha,\beta,m\neq m'}j' d^{\dagger}_{\alpha,\beta m\uparrow}d_{\alpha,\beta m'\uparrow}\langle d^{\dagger}_{\alpha,\beta m\downarrow}d_{\alpha,\beta m'\downarrow}\rangle-\sum_{\alpha,\beta,m\neq m'}j'\langle d^{\dagger}_{\alpha,\beta m\uparrow}d_{\alpha,\beta m'\uparrow}\rangle\langle d^{\dagger}_{\alpha,\beta m\downarrow}d_{\alpha,\beta m'\downarrow}\rangle$$

$$+\sum_{\alpha,\beta,m\neq m'}j\langle d^{\dagger}_{\alpha,\beta m\uparrow}d_{\alpha,\beta m'\uparrow}\rangle d^{\dagger}_{\alpha,\beta m'\downarrow}d_{\alpha,\beta m\downarrow}+\sum_{\alpha,\beta,m\neq m'}j d^{\dagger}_{\alpha,\beta m\uparrow}d_{\alpha,\beta m'\uparrow}\langle d_{\alpha,\beta m'\downarrow}d_{\alpha,\beta m\downarrow}\rangle$$

$$-\sum_{\alpha,\beta,m\neq m'}j\langle d^{\dagger}_{\alpha,\beta m\uparrow}d_{\alpha,\beta m'\uparrow}\rangle\langle d^{\dagger}_{\alpha,\beta m'\downarrow}d_{\alpha,\beta m\downarrow}\rangle.$$

If we concentrate on a homogeneous solution, the order parameters can be written as

$$\langle n^{d}_{\beta m\sigma}\rangle\equiv\langle d^{\dagger}_{\alpha,\beta m\sigma}d_{\alpha,\beta m\sigma}\rangle=\frac{1}{N}\sum_{\mathbf{k}}\langle d^{\dagger}_{\mathbf{k},\beta m\sigma}d_{\mathbf{k},\beta m\sigma}\rangle \quad (4)$$

and

$$\langle b^{d}_{\beta mm'\sigma\sigma'}\rangle\equiv\langle d^{\dagger}_{\alpha,\beta m\sigma}d_{\alpha,\beta m'\sigma'}\rangle=\frac{1}{N}\sum_{\mathbf{k}}\langle d^{\dagger}_{\mathbf{k},\beta m\sigma}d_{\mathbf{k},\beta m'\sigma'}\rangle, \quad (5)$$

which are to be determined self-consistently. We have iterated the self-consistency cycles until successive differences of all the order parameters converged to less than 2×10^{-4} by sampling 512 k points in the first Brillouin zone of the $GdFeO_3$-type structure. Typical error in the total energy is $\sim\pm0.1$ meV per formula unit cell. The HF wave function becomes a Slater determinant constructed from Bloch functions. One can calculate the single-electron excitation spectrum from the HF results by using Koopmans' theorem.

The charge-transfer energy Δ for the d^n configuration is defined as $\varepsilon_d^0-\varepsilon_p+nU$, where $U(=u-20/9j)$ is the multiplet average of the d-d Coulomb interaction. We can also define the charge-transfer energy $\Delta_{\rm eff}$ and $U_{\rm eff}$ with respect to the lowest term of each d^n configuration. The transfer integrals are given in terms of Slater-Koster parameters $(pp\sigma)$, $(pp\pi)$, $(pd\sigma)$, and $(pd\pi)$.[17] The values for Δ, U and $(pd\sigma)$ can be obtained from the cluster-model analyses of valence-band and transition-metal $2p$ core-level photoemission spectra, where systematic variation of the parameters have been revealed. The charge-transfer energy Δ increases as the atomic number of the transition metal decreases. The charge-transfer energies have been estimated to be ~1 eV for $PrNiO_3$,[18] ~3 eV for $LaFeO_3$,[19] ~4 eV for $LaMnO_3$,[19,20] ~5 eV for $LaCrO_3$ (Ref. 21), and ~6 eV for $LaTiO_3$ (Ref. 21) from the cluster-model analyses of the valence-band and transition-metal $2p$ core-level photoemission spectra. It is reasonable to interpolate and extrapolate them and to estimate the Δ for other as listed in Table I. Although the systematic variation of U is not so clear as that of Δ, U gradually decreases as the atomic number of the transition metal decreases. U have been estimated to be $\sim6-8$ eV for late transition-metal oxides[11,19,22] and ~3–5 eV for early transition-metal oxides.[21–23] The transfer integral $(pd\sigma)$ obtained from the cluster-model analyses for the transition-metal oxides are ranging from -1.0 to -2.5 eV. The values of $(pd\sigma)$ for the early transition-metal oxides with the e_g orbitals unoccupied tend to be larger than those for the late transition-metal oxides with the e_g orbitals occupied.[21,23] Based on these results, we have deduced the values of U and $(pd\sigma)$ as listed in Table 5.1. The ratio of $(pd\sigma)$ to $(pd\pi)$ is fixed to ~2, which is derived from the linear combination of atomic orbitals (LCAO) fitting of the band calculation.[24] The $(pp\sigma)$ and $(pp\pi)$ and also fixed to -0.60 and 0.15 eV, which is also taken from the LCAO fitting.[24] Ambiguity of the latter two parameters does not change the conclusion. The Kanamori parameters can be translated to Racah parameters by the relation $u=A+4B+3C$ and $j=5/2B+C$. The Racah B and C parameters are fixed to free ion values or 0.8 times of the values deduced from the atomic Hartree-Fock calculations.[25]

The $GdFeO_3$-type structure is orthorhombic with orthogonal a, b, and c axes and the unit cell contains four transition-metal ions. We have chosen the x, y, and z directions for atomic orbitals to be $(\sqrt{2}/2,\ -\sqrt{2}/2,\ 0)$, $(\sqrt{2}/2,\ \sqrt{2}/2,\ 0)$, and $(0,\ 0,\ 1)$, respectively, with respect to the a, b, and c axes. Let us denote the four sites by sites 1, 2, 3, and 4 as shown in Fig. 1(a). The $GdFeO_3$-type structure is obtained by tilting the MO_6 octahedra of cubic perovskite structure. Here, we simulate the $GdFeO_3$-type distortion by rotating the MO_6 octahedra by angle θ and $-\theta$ about the threefold axes of the octahedra or the $(0,\ -\sqrt{2}/2,\ \sqrt{2}/2)$ and $(0,\ \sqrt{2}/2,\ \sqrt{2}/2)$ axes with respect to the a, b, and c axes of the $GdFeO_3$ structure. As a result, the M-O-M bond angle

TABLE I. Parameters used for the Hartree-Fock calculations (in eV).

	Δ	U	j	$(pd\sigma)$
$R\mathrm{Ti}^{3+}\mathrm{O}_3$	7.0	4.0	0.64	−2.2
$R\mathrm{V}^{3+}\mathrm{O}_3$	6.0	4.5	0.68	−2.2
$R\mathrm{Cr}^{3+}\mathrm{O}_3$	5.0	5.0	0.72	−2.2
$R\mathrm{Mn}^{3+}\mathrm{O}_3$	4.0	5.5	0.76	−1.8
$R\mathrm{Fe}^{3+}\mathrm{O}_3$	3.0	6.0	0.80	−1.8
$R\mathrm{Co}^{3+}\mathrm{O}_3$	2.0	6.5	0.84	−1.8
$R\mathrm{Ni}^{3+}\mathrm{O}_3$	1.0	7.0	0.88	−1.8
$R\mathrm{Cu}^{3+}\mathrm{O}_3$	0.0	7.5	0.92	−1.8

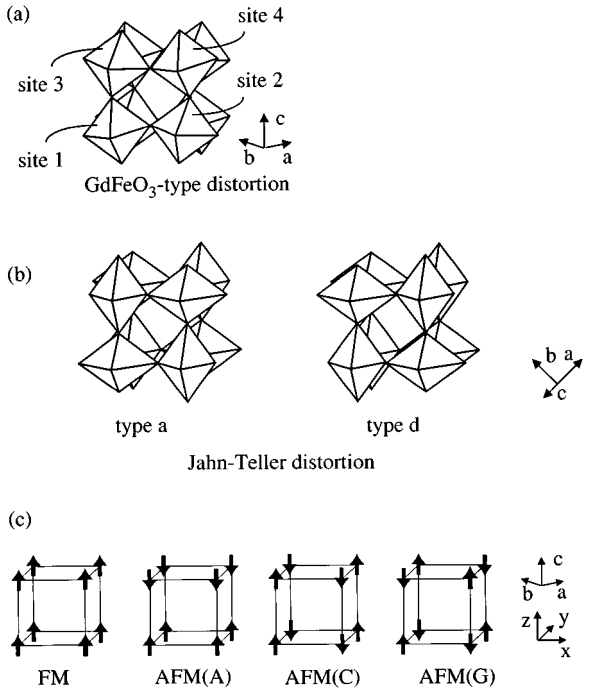

FIG. 1. (a) $GdFeO_3$-type lattice distortion. (b) Two types of Jahn-Teller lattice distortion. (c) Typical magnetic structures for the perovskites.

becomes $180-2\alpha$ [$\cos\alpha=(2/3)\cos\theta+1/3$]. In addition to the $GdFeO_3$-type distortion, some of the perovskite-type oxides show a Jahn-Teller distortion in which the MO_6 octahedra are alternatingly elongated along the x and y direction within the c plane. There are two types in the Jahn-Teller distortions as shown in Fig. 1(b) depending on the way of stacking the elongated octahedra along the c axis.[26] Basic magnetic structures for the perovskite-type transition-metal oxides are ferromagnetic (FM), A-type antiferromagnetic (AFM), C-type AFM, and G-type AFM arrangements as shown in Fig. 1(c).[27] Here, it should be noted that, in Ref. 12, the $GdFeO_3$-type distortion was simulated by rotating the MO_6 octahedra around the a axis and that only the a-type Jahn-Teller distortion was considered. In this paper, the $GdFeO_3$-type and Jahn-Teller-type distortions are included in a more realistic way.

III. RESULTS AND DISCUSSION

A. d^1 compounds

Experimentally, $LaTiO_3$, where the $GdFeO_3$-type distortion is rather small, is a G-type AFM insulator with the magnetic moment of $0.45\mu_B$, which is accompanied by weak ferromagnetism due to spin canting.[28] The optical gap of $LaTiO_3$ has been found to be ~ 0.2 eV.[29,30] More distorted $YTiO_3$ is a FM insulator with the magnetic moment of $0.84\mu_B$,[31] which has a relatively large optical gap of ~ 1 eV.[30] Their solid solution $La_{1-x}Y_xTiO_3$ is a FM insulator for $x>0.6$ and is an AFM insulator for $x<0.6$. As x goes from 1.0 to 0.0, the magnitude of the optical gap decreases from 1.0 to 0.2 eV.[31,32]

In the insulating d^1 system, one of the threefold degenerate t_{2g} orbitals should be occupied at each transition-metal site. In the cubic perovskite lattice, an electron in an orbital with a certain symmetry (xy, yz, or zx) can be transferred to that with the same symmetry at the neighboring site. Therefore, the FM state where two or three of the t_{2g} orbitals are alternatingly occupied is always favored by the intra-atomic exchange interaction j compared with the A-type, C-type, and G-type AFM states. The $GdFeO_3$-type distortion relaxes the symmetry restriction and makes it possible that an electron in an orbital with one symmetry is transferred to that with other symmetry at the neighboring site. Therefore, the distortion reduces the energy difference between the FM state and the AFM states. At this stage, we cannot explain why the less distorted $LaTiO_3$ is G-type AFM and the more distorted $YTiO_3$ is FM. In order to explain why the G-type AFM state is realized in $LaTiO_3$, we have taken account of spin-orbit interaction represented by the parameter $\zeta_d=0.018$ eV. With the spin-orbit interaction, the spins and orbitals cannot order independently. The spin-orbit interaction favors the $z'x'\uparrow+iy'z'\uparrow$ and $z'x'\downarrow-iy'z'\downarrow$ type spin orbitals, in which the spin points in the z' direction and the orbital angular momentum is antiparallel to that of the spin. A G-type AFM solution, where the two spin orbitals are alternatingly occupied with the z' axis pointing in the (1, 1, 1) direction in terms of the x, y, and z axes, is expected to be favored both by the spin-orbit interaction and by the superexchange interaction.[33] Actually the AFM solution is the lowest in energy among the solutions that we have investigated. However, the magnetic moment of the AFM state is calculated to be $\sim 0.1\mu_B$, which is too small compared with the experimental value of $LaTiO_3$. In order to resolve this discrepancy, Jahn-Teller distortion will be taken into account below.

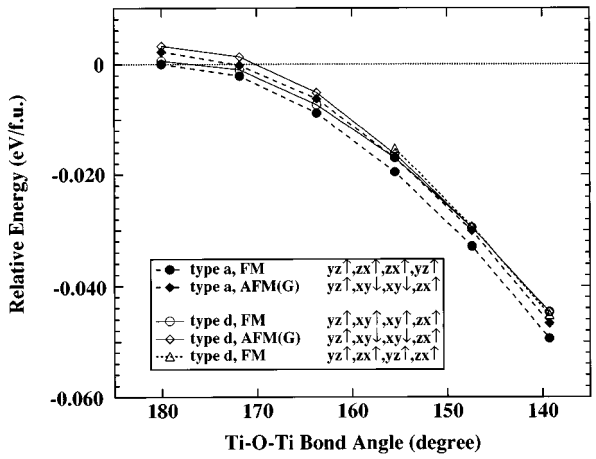

FIG. 2. Total energies of various spin and orbital arrangements for $RTiO_3$ as functions of the Ti-O-Ti bond angle.

It has been reported that $YTiO_3$ shows a Jahn-Teller distortion of the type d (Fig. 1), where the longer and shorter Ti-O bonds are ~ 2.08 and ~ 2.02 Å, respectively.[34,35] Although, in $LaTiO_3$, the difference between the longer and shorter Ti-O bonds is smaller than 0.01 Å, $LaTiO_3$ may have a small Jahn-Teller distortion of type d.[34] We have calculated the total energies of the FM and G-type AFM solutions with the Jahn-Teller distortions of types a and d (Fig. 2). Here, we have assumed that $[(pd\sigma)_s/(pd\sigma)_l]^{1/3}$, here $(pd\sigma)_s$ and $(pd\sigma)_l$ are transfer integrals for the shorter and

longer Ti-O bonds, is ~1.053. This value is somewhat larger than that estimated using the Harrison's rule[36] for $YTiO_3$, ~1.035. While the xy and yz orbitals are stabilized at sites 1 and 4 and the xy and zx orbitals are stabilized at sites 2 and 3 in the Jahn-Teller distortion of type a, xy, and yz orbitals are stabilized at sites 1 and 3 and xy and zx orbitals are stabilized at sites 2 and 4 in the Jahn-Teller distortion of type d. That is, with the Jahn-Teller distortion, one of the doubly degenerate orbitals is occupied at each site. Without the $GdFeO_3$-type distortion, an orbital ordering in which sites 1 and 4 are occupied by yz and sites 2 and 3 are occupied by zx is favored by the Jahn-Teller distortions of type a. As shown in Fig. 2, the FM solution with the orbital ordering is lower in energy than the G-type AFM solution. As the $GdFeO_3$-type distortion increases, the xy orbital is mixed into the occupied zx and yz orbitals and the energy difference between the FM and AFM solutions hardly changes. With the Jahn-Teller distortion of type d, a FM solution with the yz, xy, xy, zx-type orbital ordering, in which sites 1, 2, 3, and 4 are occupied by yz, xy, xy, and zx, respectively, is the lowest in energy when the $GdFeO_3$-type distortion is small. As the $GdFeO_3$-type distortion increases, the energy difference between the FM and AFM solutions with the yz, xy, xy, zx-type orbital ordering decreases and the two become almost degenerate in energy for $\angle$Ti-O-Ti=147.4°, as shown in Fig. 2. On the other hand, FM and AFM solutions with the orbital ordering in which sites 1 and 4 are occupied by yz and sites 2 and 3 are occupied by zx are unstable without the $GdFeO_3$-type distortion. As the $GdFeO_3$-type distortion increases, the xy orbital is mixed into the occupied zx and yz orbitals and these solutions are strongly stabilized. As a result, the FM and AFM solutions in which sites 1, 2, 3, and 4 are occupied by c_1yz+c_2xy, c_1zx+c_2xy, c_1yz-c_2xy, and $c_1zx-c_2xy(c_1^2+c_2^2=1)$, respectively, become lower in energy than the FM and AFM solutions with the yz-, xy-, xy-, zx-type orbital ordering for $\angle$Ti-O-Ti=139.3°. Here, c_1 is ~0.8 and c_2 is ~0.6. In $YTiO_3$, with $\angle$Ti-O-Ti of ~140° and the d-type Jahn-Teller distortion, the orbital ordering, in which sites 1, 2, 3, and 4 are occupied by c_1yz+c_2xy, c_1zx+c_2xy, c_1yz-c_2xy, and c_1zx-c_2xy $(c_1^2+c_2^2=1)$, respectively, may be realized. This type of orbital ordering has also been found in the *ab initio* band-structure calculation for $YTiO_3$, using the generalized-gradient approximation.[37]

In Fig. 3, we have plotted the energy difference between the FM and G-type AFM solutions with the above orbital ordering and the magnetic moment of the two solutions as functions of the magnitude of the Jahn-Teller distortion of type d. While the G-type AFM state has a lower energy than the FM state for $\angle$Ti-O-Ti~155.5°, the FM solution is lower in energy than the G-type AFM solution for $\angle$Ti-O-Ti~139.3°. This explains why the less distorted $LaTiO_3$ is AFM and the more distorted $YTiO_3$ is FM. With the Jahn-Teller distortion $[(pd\sigma)_s/(pd\sigma)_l]^{1/3}\sim1.053$, the orbital angular momentum is now almost quenched and the magnetic moment becomes $\sim0.85\mu_B$, which is in good agreement with the experimental value of $YTiO_3$. As the Jahn-Teller distortion decreases, the magnetic moment of the G-type and FM solutions become smaller. With

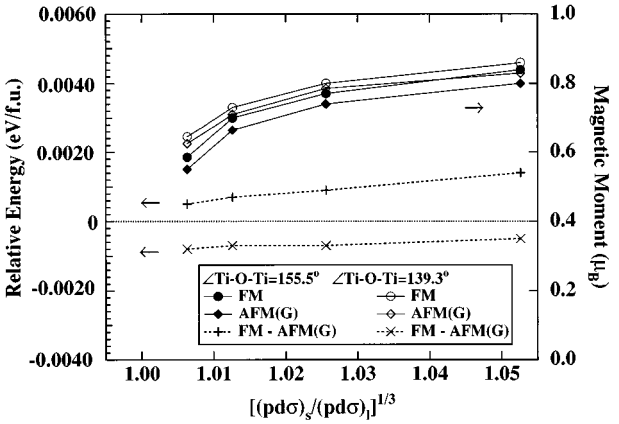

FIG. 3. Energy difference between the FM and G-type AFM solutions and the magnetic moment of the two solutions for $RTiO_3$ as functions of the Jahn-Teller lattice distortion of type d.

$[(pd\sigma)_s/(pd\sigma)_l]^{1/3}\sim1.006$, the magnetic moment of the G-type AFM state is calculated to be $\sim0.55\mu_B$ for $\angle$Ti-O-Ti~155.5°, which is reduced from $1\mu_B$, because of the spin-orbit coupling and agrees with the experimental value of $LaTiO_3$.[28]

Thus the present HF calculation presents us the following scenario to explain the difference between AFM $LaTiO_3$ and FM $YTiO_3$: The $GdFeO_3$ distortion stabilizes the FM state with the orbital ordering compared with the AFM state, which causes the Jahn-Teller distortion. The problem is why the Jahn-Teller distortion of type d is realized in $YTiO_3$ instead of the type a. The HF calculation cannot provide an answer to this question. In $Y_{1-x}Ca_xTiO_3$, the FM spin-ordering disappears $x>0.1$ and the insulator-to-metal transition occurs at $x=0.4$.[38] The PM insulating region ranging from $x=0.1$ to $x=0.4$ may be attributed to a spin-disordered and orbital-ordered state. On the other hand, spin and orbital orderings are strongly coupled through the spin-orbit interaction in $LaTiO_3$. This is consistent with the fact that the AFM to PM transition and the insulator-metal transition occur at the same composition in $La_{1-x}Sr_xTiO_3$.[38]

In Fig. 4, the density of states for the FM and AFM solutions is shown. The band gap opens between the occupied and unoccupied t_{2g} orbitals, the magnitude of which is mainly determined by $u'-j$. From the HF calculation, the magnitudes of the band gaps for the FM and G-type AFM solutions are estimated to be ~2.7 and ~2.8 eV, respectively, which are considerably larger than the experimental values.[29,30] The magnitude of the band gap for the FM and G-type AFM states is hardly changed by the distortion, contradicting the experimental results.[29,30] In the present HF calculation, since the $GdFeO_3$-type distortion makes some e_g character hybridize into the t_{2g} band, the distortion does not necessarily decrease the bandwidth and increase the band gap as expected from a simple model where only a single t_{2g} orbital is considered.[29] This discrepancy between the calculated and experimental band gaps may indicate the limitation of the HF approximation and the breakdown of Koopmans' theorem.

B. d^2 compounds

$LaVO_3$ has a structural and magnetic phase transition at ~140 K. Below the transition temperature, the C-type AFM

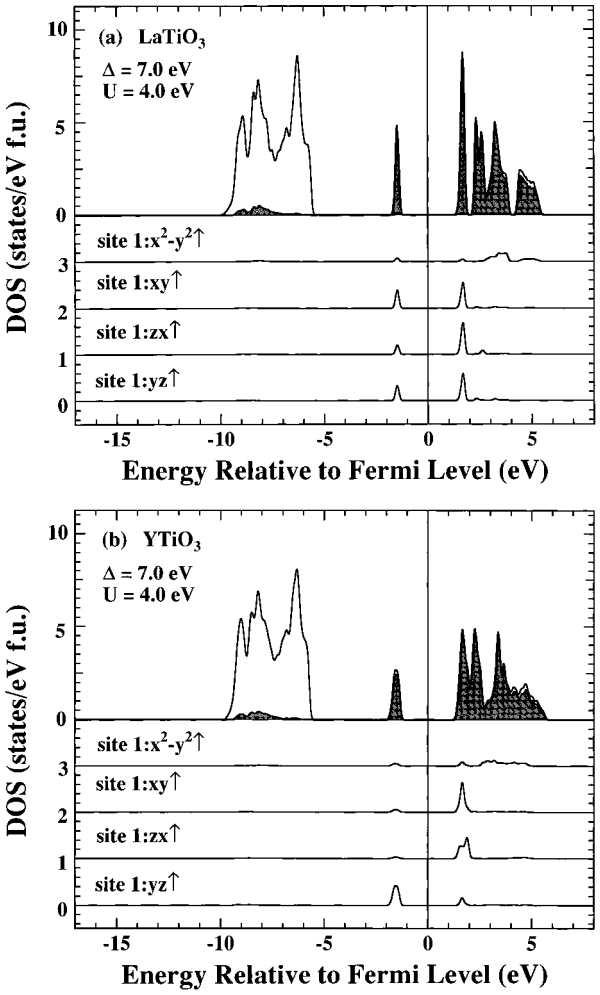

FIG. 4. Density of states for (a) $LaTiO_3$ and (b) $YTiO_3$. The shaded area indicates the transition-metal $3d$ weight. The x^2-y^2, xy, zx, and yz components at site 1 are shown in the lower panel.

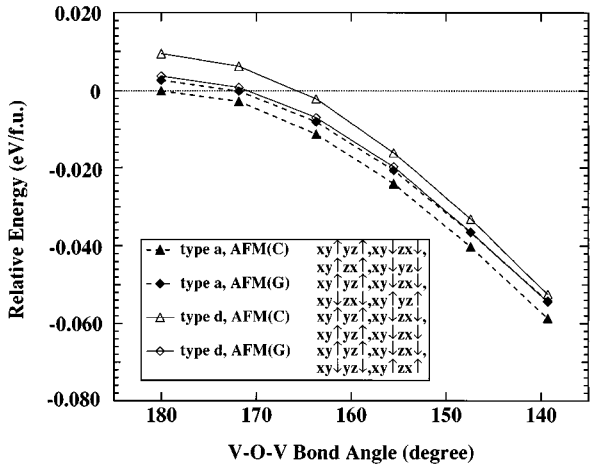

FIG. 5. Total energies of various spin and orbital arrangements for RVO_3 as functions of the V-O-V bond angle.

magnetic ordering with the magnetic moment $\sim 1.3\mu_B$ is realized and a distortion from the orthorhombic $GdFeO_3$-type structure to a monoclinic one occurs.[39] The distortion can be viewed as a Jahn-Teller distortion of type a. $LaVO_3$ is an insulator with an optical gap of ~ 1.1 eV.[30] YVO_3, which has a larger $GdFeO_3$-type distortion than $LaVO_3$, and is accompanied by a Jahn-Teller distortion of type d. The magnetic structure of YVO_3 is G-type AFM with the magnetic moment of $\sim 1.6\mu_B$ below 77 K and is C type with the magnetic moment of $\sim 1.0\mu_B$ between 77 and 118 K.[40] YVO_3 is also an insulator with an optical gap of ~ 1.8 eV.[30]

In the d^2 compounds, since two of the t_{2g} orbitals should be occupied at each site, a possible orbital ordering is that in which one of the t_{2g} orbitals is occupied in all the sites and the other two are alternatingly occupied. Previously, this type of the orbital ordering has been investigated in V_2O_3.[7,8] Without the Jahn-Teller and $GdFeO_3$-type distortions, the HF calculation predicts that the C-type AFM state with the orbital ordering where a site with the xy and yz orbitals occupied and one with the xy and zx orbitals occupied are alternatingly arranged, is the lowest state. The reason why the C-type AFM spin arrangement is favored by this orbital ordering is as follows. Since the xy orbital is occupied in all the sites, the superexchange interactions along the x and y directions are AFM. On the other hand, the superexchange interaction along the z direction, which is mainly determined by the transfer of the electrons with the zx and yz symmetry, is FM because the zx and yz orbitals are alternatingly occupied along the z direction.

When the spin-orbit interaction of $\zeta_d = 0.025$ eV is included, the $zx\uparrow + iyz\uparrow$ and $zx\downarrow - iyz\downarrow$ type spin orbitals are favored as discussed in the previous section.[16] Consequently, a G-type AFM solution where the two are alternatingly occupied and the xy orbital is occupied in all the sites becomes lower in energy than a C-type AFM solution. The energy difference between the G-type and C-type AFM states becomes smaller as the $GdFeO_3$-type distortion increases.

With the Jahn-Teller distortion of type a, the orbital ordering where a site with xy and yz occupied and one with xy and zx occupied are alternatingly arranged is regained. Therefore, the C-type AFM solution is lower in energy than the G-type AFM solution with the Jahn-Teller distortion of type a as shown in Fig. 5. Here, we have assumed that $[(pd\sigma)_s/(pd\sigma)_l]^{1/3}$, where $(pd\sigma)_s$ and $(pd\sigma)_l$ are transfer integrals for the shorter and longer V-O bonds, is ~ 1.053. This value is somewhat larger than those estimated using the Harrison's rule,[36] ~ 1.035 for $LaVO_3$ and ~ 1.04 for YVO_3. The calculated result can explain why $LaVO_3$ accompanied by the a-type distortion is C-type AFM. On the other hand, in the orbital ordering driven by the Jahn-Teller distortion of type d, the same pair of orbitals is occupied along the c axis and the FM spin coupling along the c axis is not favored. Therefore, with the Jahn-Teller distortion of type d, the G-type AFM solution is lower in energy than the C-type AFM solution, which agrees with the experimental result that YVO_3 with the d-type Jahn-Teller distortion shows G-type AFM. However, in the present calculation, the energy gain by the a-type Jahn-Teller distortion is larger than that by the d-type irrespective of the magnitude of the $GdFeO_3$-type lattice distortion, as shown in Fig. 5. The HF calculation fails to explain why the less distorted $LaVO_3$ has the Jahn-Teller distortion of type a and the more distorted YVO_3 shows the Jahn-Teller distortion of type d. In the d^1 system, the more distorted $YTiO_3$ is also accompanied by the Jahn-Teller distortion of type d. In order to explain why

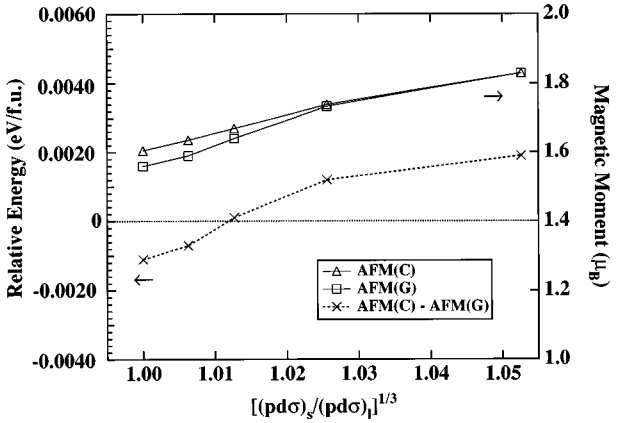

FIG. 6. Energy difference between the C-type and G-type AFM solutions and the magnetic moment of the two solutions for $R\mathrm{VO}_3$ as functions of the Jahn-Teller lattice distortion of type d.

the d-type Jahn-Teller distortion is realized in YVO_3, we have to assume that the GdFeO_3-type lattice distortion favors the Jahn-Teller distortion of type d compared with that of type a.

The magnetic moment at the V site is calculated to be $\sim 1.8\mu_B$ for the C-type AFM state with the a-type Jahn-Teller distortion and the G-type AFM state with the d-type Jahn-Teller distortion. This value is in good agreement with the experimental value for the G-type AFM state in YVO_3, but is much larger than those observed for the C-type AFM states in YVO_3 and LaVO_3. In Fig. 6, we have plotted the energy difference between the C-type and G-type AFM solutions and the magnetic moment of the two solutions as functions of the magnitude of the d-type Jahn-Teller distortion for $\angle$V-O-V$\sim 139.3°$. As the Jahn-Teller distortion decreases, the energy difference between the C-type and G-type AFM states and the magnetic moment of the two solutions decrease. Without the Jahn-Teller distortion, the C-type AFM solution is lower in energy than the G-type AFM solution and the calculated magnetic moment is $\sim 1.5\mu_B$ for the C-type AFM state, which is close to the experimental value for the C-type AFM states in YVO_3 and LaVO_3. This result suggests that the transition from the G-type AFM state to the C-type one in YVO_3 may be related to the reduction of the Jahn-Teller distortion.

In Fig. 7, the density of state for the C-type and G-type AFM solutions is shown. The band gap opens between the occupied and unoccupied t_{2g} orbitals, the magnitude of which is mainly determined by $u'-j$. The character of the band gap is of the typical Mott-Hubbard type. From the HF calculation, the magnitudes of the band gaps for the C-type AFM and G-type AFM solutions are found to be ~ 3.3 and ~ 3.4 eV, respectively, which are by 1–2 eV larger than the experimental results,[30] indicating the limitation of the HF approximation. Recently, Sawada, Hamada, and Terakura[41] have performed *ab initio* band-structure calculations for YVO_3 and LaVO_3, using the generalized gradient approximation, which correctly predict the spin and orbital ordering for LaVO_3. In contrast to the present model HF result, the magnitude of the band gap is underestimated in the generalized-gradient-approximation calculation.

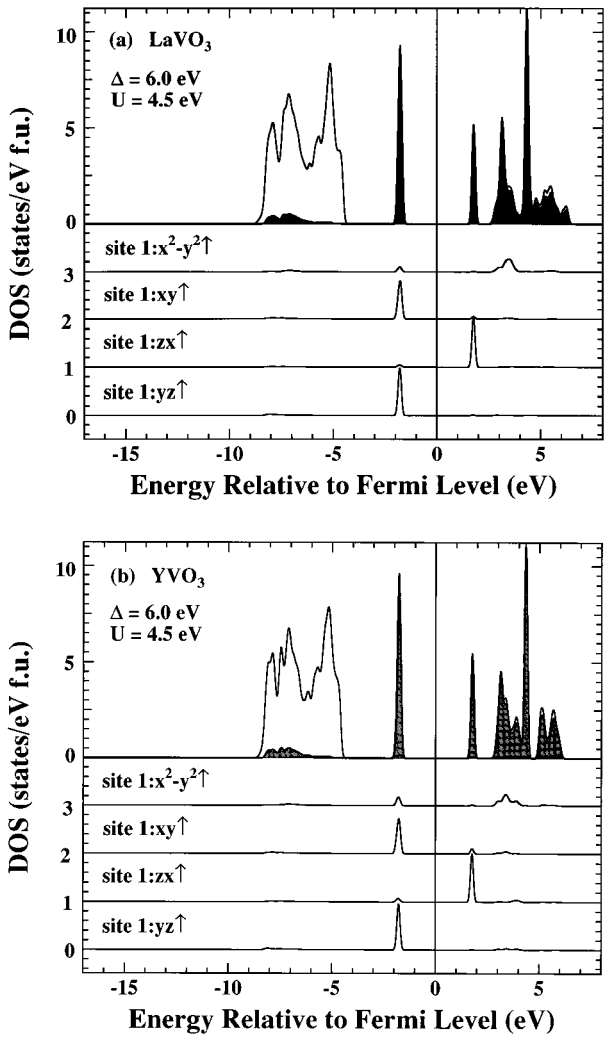

FIG. 7. Density of states for (a) LaVO_3 and (b) YVO_3. The shaded area indicates the transition-metal $3d$ weight. The x^2-y^2, xy, zx, and yz components at site 1 are shown in the lower panel.

C. d^3 compounds

In high-spin d^3 compounds, where the t_{2g} orbitals are half filled, there is no orbital degree of freedom. Therefore, the G-type AFM state is expected to have the lowest energy. Actually, the G-type AFM solution is the lowest for the parameter set appropriate for LaCrO_3. Experimentally, LaCrO_3 is a G-type AFM insulator with the magnetic moment of $\sim 2.8\mu_B$ (Ref. 42) and with the optical gap of ~ 3.5 eV.[30] The calculated magnetic moment is $\sim 3.0\mu_B$, in good agreement with the experimental value. In Fig. 8, the density of states for LaCrO_3 is shown. The magnitude of the band gap is calculated to be ~ 4.5 eV, which is also larger than the experimental value by ~ 1 eV, as in the Ti and V oxides. The character of the band gap is of the Mott-Hubbard type. However, a large amount of oxygen $2p$ character is mixed into the $3d$ orbitals just above and below the band gap compared with LaTiO_3 and LaVO_3, implying a crossover from the Mott-Hubbard regime to the charge-transfer regime with atomic number.

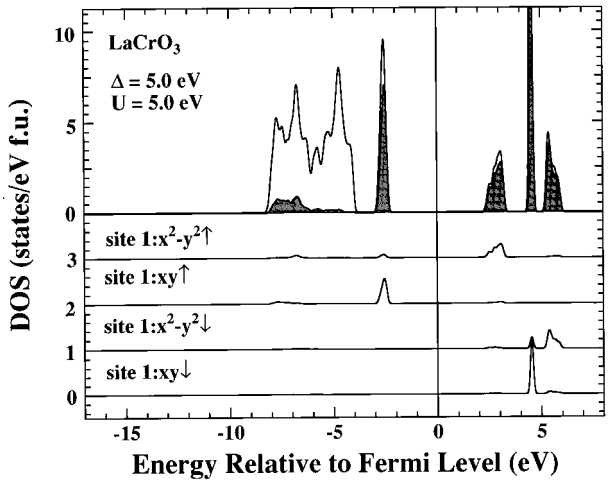

FIG. 8. Density of states for $LaCrO_3$. The shaded area indicates the transition-metal $3d$ weight. The x^2-y^2, xy, zx, and yz components at site 1 are shown in the lower panel.

D. d^4 compounds

In d^4 high-spin compounds, one of the e_g orbitals is occupied and there is also interesting interplay between the orbital ordering and the Jahn-Teller distortion. The Mn^{3+} perovskite-type oxide $LaMnO_3$ is accompanied by a Jahn-Teller distortion of type d and is an A-type AFM insulator with the magnetic moment of $\sim 3.7\mu_B$.[27,43] It is possible to estimate the effect of the Jahn-Teller distortion by scaling the transfer integrals with respect to the distance between the transition-metal ion and the oxygen ion. The magnitude of the Jahn-Teller distortion is again represented by the ratio $(pd\sigma)_s/(pd\sigma)_l$.

Without the Jahn-Teller distortion, the HF calculation gives us two types of A-type AFM insulating solutions accompanied by the $3x^2$-$r^2/3y^2$-r^2-type orbital ordering with a considerable mixture of $3z^2$-r^2, which can be regarded as a mixture of the $3x^2$-$r^2/3y^2$-r^2-type and z^2-x^2/z^2-y^2-type orbital orderings.[4,44] One has the orbital arrangement compatible with the d-type Jahn-Teller distortion, in which sites 1 and 3 are occupied by $(1/\sqrt{2})(3z^2\text{-}r^2)+(1/\sqrt{2})(x^2\text{-}y^2)$ and sites 2 and 4 are occupied by $(1/\sqrt{2})(3z^2\text{-}r^2)\text{-}(1/\sqrt{2})\times(x^2\text{-}y^2)$, and the other has that compatible with the a-type Jahn-Teller distortion, in which sites 1 and 4 are occupied by $(1/\sqrt{2})(3z^2\text{-}r^2)+(1/\sqrt{2})(x^2\text{-}y^2)$ and sites 2 and 3 are occupied by $(1/\sqrt{2})(3z^2\text{-}r^2)\text{-}(1/\sqrt{2})(x^2\text{-}y^2)$. The two solutions are exactly degenerate in energy.[4] We can also obtain two types of FM insulating states. One is accompanied by the orbital ordering in which sites 1, 2, 3, and 4 are occupied by z^2-y^2, $3x^2$-r^2, $3y^2$-r^2, and z^2-x^2 orbitals, respectively, and the other is by that in which sites 1, 2, 3, and 4 are occupied by z^2-y^2, $3x^2$-r^2, $3x^2$-r^2, and z^2-y^2 orbitals, respectively. As shown in Fig. 9, the former FM solution consistent with the d-type Jahn-Teller distortion is lower in energy and has a larger band gap than the latter one compatible with the a-type Jahn-Teller distortion. The total energies of the FM solutions are lower than those of the A-type AFM solutions. This is because FM coupling is favored both in the a-b plane and between the a-b planes, due to the orbital ordering.

A small Jahn-Teller distortion makes the two FM solutions almost degenerate in energy and turns the orbital orderings of the two into the $3x^2$-$r^2/3y^2$-r^2-type orbital ordering with a mixture of $3z^2$-r^2, which is the same as that found in the A-type AFM solutions. The magnitude of the band gap for the FM solution compatible with the d-type Jahn-Teller distortion is reduced and becomes almost equal to that for the FM solution compatible with the a-type Jahn-Teller distortion, as shown in Fig. 9. Although the energy difference between the FM and A-type AFM solutions becomes smaller, the FM solutions are still lower in energy than the A-type AFM solutions.

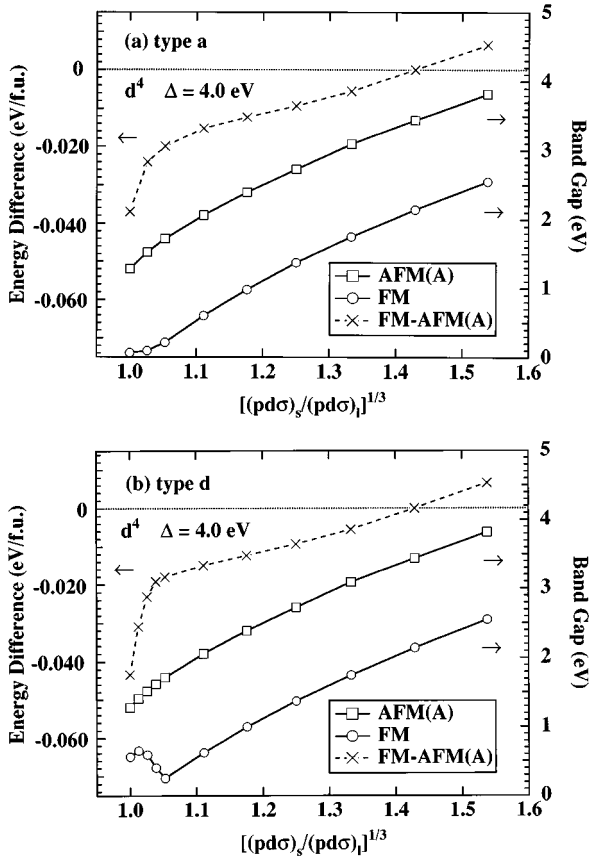

FIG. 9. Energy difference between the FM and A-type AFM states and the band gaps of the FM and A-type AFM states for $LaMnO_3$ as a function of the Jahn-Teller lattice distortion (a) of type a and (b) of type d.

As the Jahn-Teller distortion increases, the orbital ordering becomes purely of the $3x^2$-$r^2/3y^2$-r^2-type. As a result, AFM coupling between the a-b planes becomes more favored than FM coupling and the A-type AFM solution is strongly stabilized, as shown in Fig. 9. The calculated magnetic moment of the A-type AFM state is $\sim 3.9\mu_B$ for $[(pd\sigma)_s/(pd\sigma)_l]^{1/3}=1.43$, which agrees with the experimental value. This indicates that the disappearance of the Jahn-Teller distortion by hole doping turns A-type AFM into a FM arrangement. Actually, in $La_{1-x}Sr_xMnO_3$, the Jahn-Teller distortion is suppressed by hole doping and the system becomes FM.[45] Figure 9 also shows that the magnitude of the band gap of the FM state is smaller than that of the A-type AFM state, indicating that the metallization in $La_{1-x}Sr_xMnO_3$ by hole doping is favored by the changes in the spin and orbital ordering.

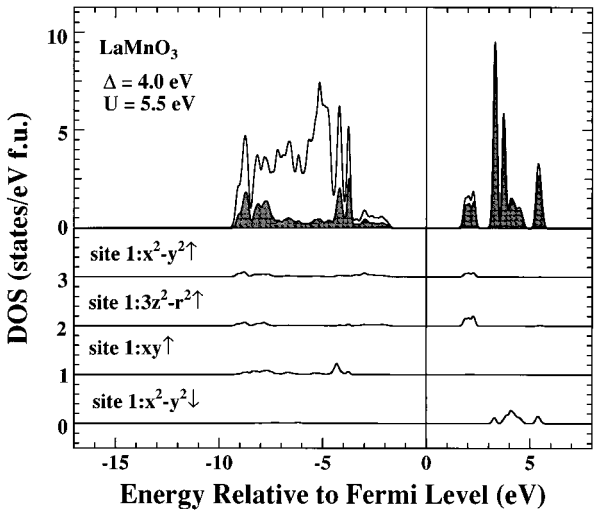

FIG. 10. Density of states for $LaMnO_3$. $[(pd\sigma)_s/(pd\sigma)_l]^{1/3}=1.43$. The shaded area indicates the transition-metal $3d$ weight. The x^2-y^2, xy, zx, and yz components at site 1 are shown in the lower panel.

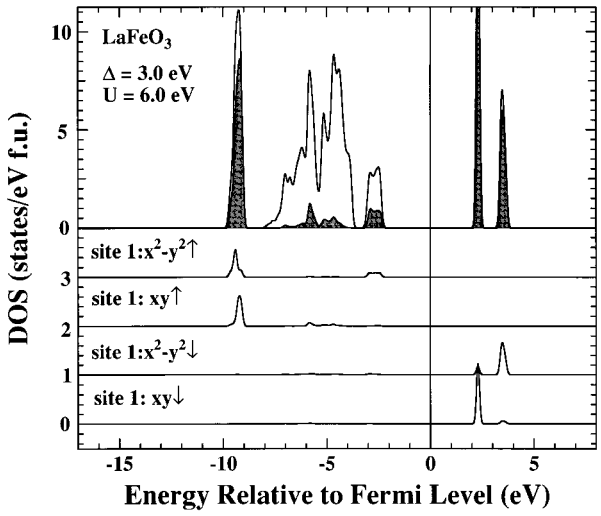

FIG. 11. Density of states for $LaFeO_3$. The shaded area indicates the transition-metal $3d$ weight. The x^2-y^2, xy, zx, and yz components at site 1 are shown in the lower panel.

In Fig. 10, the density of states for the A-type AFM solution is shown. The band gap opens between the occupied and unoccupied e_g orbitals. In contrast to $LaTiO_3$ and $LaVO_3$, $LaMnO_3$ falls into the charge-transfer regimes. Therefore, the magnitude of the band gap is mainly determined by Δ. However, a large amount of Mn $3d$ character is mixed into the states just above and below the Fermi level and the character of the band gap deviates from the typical charge-transfer type or the p-d type. As shown in Fig. 9, the magnitude of the band gap of the A-type AFM state increases as the Jahn-Teller distortion increases. The magnitudes of the band gap for the A-type AFM solution with the Jahn-Teller distortion, which makes the A-type AFM solution lower in energy than the FM solution, is calculated to be $\sim$3 eV, which is larger than the experimental value $\sim$1.3 eV.[30,46]

E. d^5 compounds

High-spin d^5 compounds, where t_{2g} orbitals are half filled, have no orbital degree of freedom. Therefore, the G-type AFM state has the lowest energy in the HF calculation. Experimentally, $LaFeO_3$ is a G-type AFM insulator with the magnetic moment of $\sim 4.6\mu_B$ (Ref. 42) and with the optical gap of $\sim$2.5 eV.[30] The calculated magnetic moment is $\sim 4.6\mu_B$ and is in good agreement with the experimental value. In Fig. 11, the density of states for $LaFeO_3$ is shown. The magnitude of the band gap is estimated to be $\sim$4 eV, which is larger than the experimental value by $\sim$1.5 eV. The character of the band gap is of the charge-transfer type.

F. d^6 compounds

$LaCoO_3$ is a nonmagnetic insulator, where the t_{2g} orbitals are fully occupied and there is no orbital degree of freedom. However, the magnetic susceptibility studies of $LaCoO_3$ indicate that the nonmagnetic-to-paramagnetic transition occurs at $\sim$90 K,[47] which can be regarded as a transition from the low-spin $t_{2g\uparrow}^3 t_{2g\downarrow}^3$ configuration to the intermediate-spin $t_{2g\uparrow}^3 t_{2g\downarrow}^2 e_{g\uparrow}$ or high-spin $t_{2g\uparrow}^3 t_{2g\downarrow} e_{g\uparrow}^2$ configurations. Therefore, it is interesting to study the effect of orbital ordering in the intermediate- and high-spin states. For the intermediate-spin and high-spin states, FM metallic, and G-type AFM insulating solutions are the lowest in energy, respectively, according to the HF calculation. The low-spin state, where the e_g orbitals are mixed into the t_{2g} orbitals through the j' term, is lower in energy by $\sim$0.15 eV per formula unit cell than that without the t_{2g}-e_g mixing. However, since the energy gain due to the j' term is underestimated in the HF approximation, the HF calculation fails to give the energy difference between the states with different total spins. Actually, for the parameter set listed in Table I, the high-spin state is much lower in energy than the low-spin state, although the low-spin and high-spin states are almost degenerate in the configuration-interaction cluster-model calculation.[48]

Here, tentatively, the relative energies of the intermediate- and high-spin states to the low-spin state are calculated as

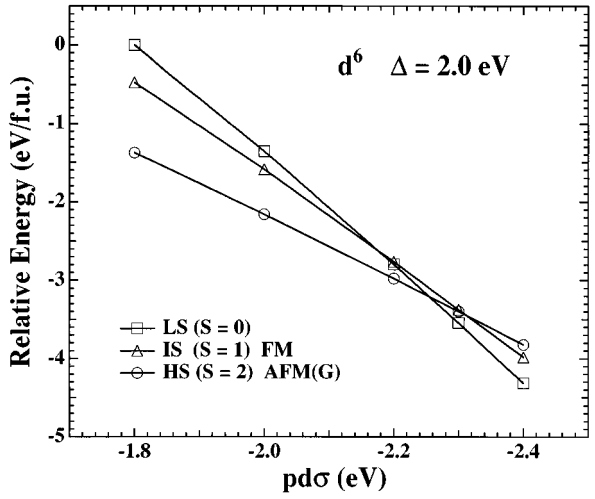

FIG. 12. Total energies of the low-, intermediate-, and high-spin solutions for $LaCoO_3$ as functions of $(pd\sigma)$.

functions of $(pd\sigma)$ as shown in Fig. 12. In order to make the low-spin state lower in energy than the high-spin state, $|(pd\sigma)|$ should be larger than 2.3 eV. For $(pd\sigma)<-2.3$ eV, the low-spin state is the lowest and the intermediate-spin state is the second lowest, suggesting that the intermediate-spin state may play an important role in the nonmagnetic-to-paramagnetic transition observed in $LaCoO_3$. Recently, Korotin *et al.* have found that the total energy of the FM intermediate-spin state is lower than that of the high-spin state by applying the LDA+U method to $LaCoO_3$ and have pointed out the importance of orbital ordering in the intermediate-spin state.[49] In our calculation, for $\Delta=2.0$ eV, the intermediate-spin state is metallic and has no orbital ordering. However, for $\Delta=3.0$ eV, we can obtain a FM insulating state with the orbital ordering where sites 1, 2, 3, and 4 are occupied by z^2-y^2, $3x^2$-r^2, $3y^2$-r^2, and z^2-x^2 orbitals, respectively. This orbital ordering is the same as that found in the FM solution for $LaMnO_3$.

The magnetic moment of the intermediate-spin and high-spin states are calculated to be $\sim 2.2\mu_B$ and $\sim 3.5\mu_B$, respectively. Since the magnetic moment observed in the FM metallic phase of $La_{1-x}Sr_xCoO_3$ is ~ 1–$2\mu_B$,[47] the intermediate-spin FM solution may also be closely related to the FM metallic state in the $La_{1-x}Sr_xCoO_3$ system.

In Fig. 13, the density of states for the low-, intermediate-, and high-spin states are shown. The magnitude of the band gap of the low-spin state is calculated to be ~ 3.5 eV, which is considerably overestimated compared with the experimental value ~ 0.6 eV.[30,50] Whereas the parameter set for $LaCoO_3$ falls in the charge-transfer regime, the Co $3d$ and O $2p$ orbitals are strongly hybridized for states just below the Fermi level in the low-spin state. On the other hand, the character of the band gap in the high-spin state is of the typical charge-transfer type. The density of states for the low-, intermediate-, and high-spin states are quite different. Therefore, it may be interesting to compare the three calculated results with the photoemission and inverse-photoemission spectra of $LaCoO_3$ and $La_{1-x}Sr_xCoO_3$.[48,50]

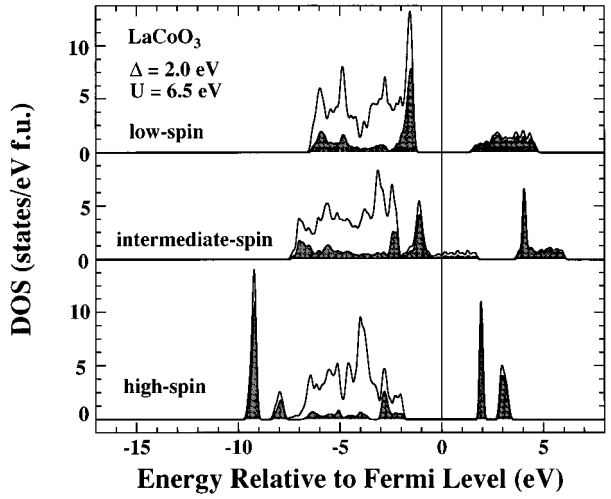

FIG. 13. Density of states of the low-, intermediate-, and high-spin solutions for $LaCoO_3$. The shaded area indicates the transition-metal $3d$ weight.

G. d^7 compounds

In the Ni^{3+} (low-spin d^7) perovskite-type oxides, the least distorted $LaNiO_3$ is a PM metal and more distorted $RNiO_3$ with the R ion smaller than La are AFM insulators.[51] $PrNiO_3$ and $NdNiO_3$ show unusual magnetic structures, the unit cell of which includes 16-Ni ions and in which each Ni ion is ferromagnetically coupled to three-nearest neighbors and antiferromagnetically coupled to the other three.[52] In order to explain this magnetic structure, García-Muñoz, Rodríguez-Carvajal, and Lacorre have proposed that the e_g orbitals are polarized into $3z^2$-r^2 and x^2-y^2 for the ferromagnetically coupled Ni pairs and are polarized into the same orbitals for the antiferromagnetically coupled Ni pairs.[52] However, in Ref. 15, we have performed the HF calculation for the actual magnetic structure with possible orbital orderings and have found that the solutions with the observed magnetic structure is higher in energy than the FM and A-type AFM solutions. Here, we present the results for the FM and A-type, C-type, and G-type AFM states in detail, which may give us a clue to find another possible spin- and orbital-ordered state compatible with the experimental result. As discussed in Ref. 12, for $\Delta=1.0$ eV, the high-spin AFM insulating state is lower in energy than the low-spin states and the low-spin FM state, which is the lowest in energy among the low-spin solutions, is metallic. This discrepancy may be due to the lack of ''Heitler-London-type'' or $(\uparrow\downarrow-\downarrow\uparrow)$-type electron correlation between the $3d$ electron and the oxygen $2p$ hole with antiparallel spins in the HF ground state. We present below the results for $\Delta=2.0$ eV, where all the low-spin insulating solutions exist as metastable states, in order to show the relationship between the spin and orbital orderings more clearly. Since, in the low-spin d^7 system, the t_{2g} orbitals mix with the e_g orbitals through the off-diagonal Coulomb j' terms as in the low-spin d^6 system, we denote the e_g orbitals which have mixtures of t_{2g} orbitals as ''$3z^2$-r^2'' and ''x^2-y^2.'' The FM and C-type AFM solutions, which have FM coupling along the c axis, favors the ''$3z^2$-r^2''/''x^2-y^2''-type orbital ordering. In the FM solution, sites 1, 2, 3, and 4 are occupied by ''z^2-y^2,'' ''$3x^2$-r^2,'' ''$3y^2$-r^2,'' and ''z^2-x^2'' orbitals. This orbital ordering is similar to that obtained for the FM state in $LaMnO_3$. In the C-type AFM solution, sites 1, 2, 3, and 4 are occupied by ''x^2-y^2,'' ''x^2-y^2,'' ''$3z^2$-r^2,'' and ''$3z^2$-r^2'' orbitals. On the other hand, the A-type and G-type AFM solutions have the ''$3x^2$-r^2''/''$3y^2$-r^2''-type orbital ordering. Namely, in the A-type and G-type AFM solutions, sites 1, 2, 3, and 4 are occupied by ''$3y^2$-r^2,'' ''$3x^2$-r^2,'' ''$3y^2$-r^2,'' and ''$3x^2$-r^2'' orbitals into which ''$3z^2$-r^2'' is mixed. This orbital ordering is essentially the same as that found in the A-type AFM solution for $LaMnO_3$. The total energies of the various solutions for $\Delta=2.0$ eV are plotted in Fig. 14 as functions of the Ni-O-Ni bond angle. The FM solution and the A-type AFM solution are very close in energy to each other, suggesting that complicated magnetic structures, where both the FM coupling and AFM coupling coexist and the FM coupling within the a-b plane and that between the a-b planes are competing, may be realized in these compounds. In Fig. 14, the band gaps for these solutions are also plotted as functions of the Ni-O-Ni bond angle. As the bond

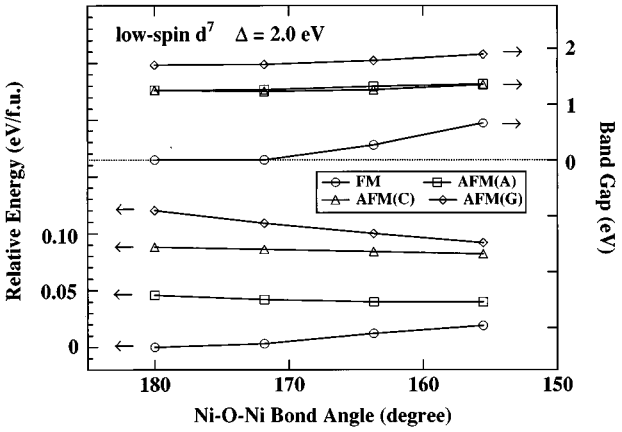

FIG. 14. Total energies and the band gaps of various spin and orbital arrangements for the $R\mathrm{NiO}_3$ system as functions of the Ni-O-Ni bond angle.

angle decreases, the band gaps increases for any spin- and orbital-ordered structures, which is essentially the same as the result in Ref. 12 and explains the increase of the metal-insulator transition temperature in going from PrNiO_3 to NdNiO_3.[51]

In Fig. 15, the density of states for the high-spin G-type AFM, low-spin A-type AFM, FM, and PM solutions are shown for $\Delta=1.0$ eV and $\angle$Ni-O-Ni$=180°$. In the low-spin A-type AFM states, the band gap opens between the occupied e_g-type orbitals, which mainly has O $2p$ character, and the unoccupied e_g-type orbitals, in which Ni $3d$ character is dominant. Therefore, the character of the band gaps is of the charge-transfer type in the HF calculation. The band gap of the high-spin G-type AFM state is also of the charge-transfer type. Since the dispersions of the energy bands consisting of the e_g-type orbitals are very strong in the low-spin state, the magnitude of the band gap of the low-spin A-type AFM state

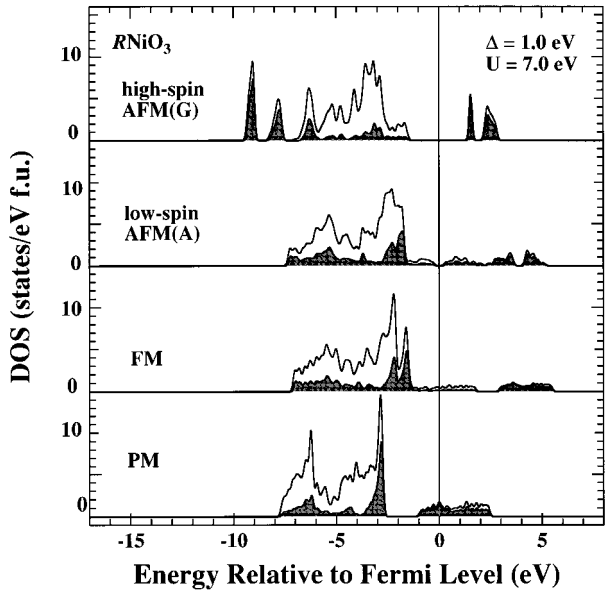

FIG. 15. Density of states of the high-spin G-type AFM, low-spin A-type AFM, FM, and PM solutions for $R\mathrm{NiO}_3$. The shaded area indicates the transition-metal $3d$ weight.

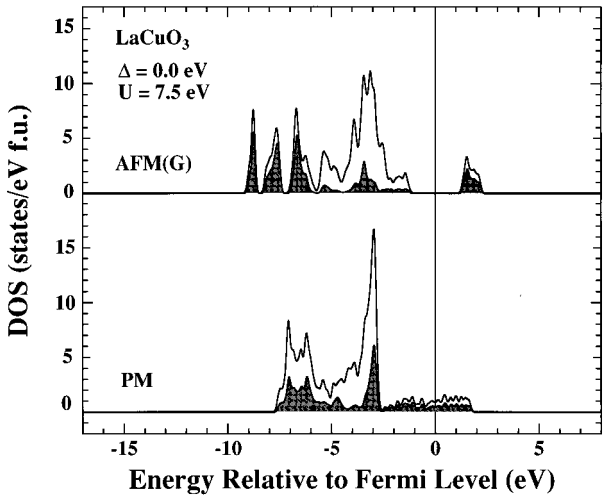

FIG. 16. Density of states of the G-type AFM and PM solutions for LaCuO_3. The shaded area indicates the transition-metal $3d$ weight.

is much smaller than that of the high-spin G-type AFM state. In the FM and PM states, the e_g-type bands with the width of ~ 3 eV, in which the Ni $3d$ and O $2p$ orbitals are strongly hybridized, cross the Fermi level. The e_g-type bands are half filled and quarter filled for the FM and PM solution, respectively. As mentioned above, the FM metallic state is the second lowest among the four solutions and the PM metallic state is much higher in energy than the FM state. However, experimentally, the metal-insulator transition of the $R\mathrm{NiO}_3$ system as a function of the size of the R ion is that from a PM metal to an AFM insulator and there is no region in which a FM metallic state is realized.[50] This discrepancy is considered to be due to the lack of spin and orbital fluctuations in the HF approximation. The energy of the PM metallic state may significantly be lowered by the inclusion of spin and orbital fluctuations beyond the HF approximation compared with the other spin- and orbital-ordered states.

H. d^8 compounds

In high-spin d^8 compounds, where the t_{2g} orbitals are fully occupied and the e_g orbitals are half filled, there is no orbital degree of freedom because the high-spin state is always realized in the octahedral coordination. Therefore, the G-type AFM state is the lowest in energy in the HF calculation. This result is consistent with the LDA$+U$ calculation by Czyzyk and Sawatzky, which predict tetragonally distorted LaCuO_3 as an insulator with the G-type AFM ordering.[53] However, experimentally, rhombohedrally distorted LaCuO_3 is a PM metal and the tetragonally distorted LaCuO_3 also shows metallic behavior.[54] As mentioned in the previous section, the HF calculation fails to describe the PM metallic state near the metal-insulator transition. The energy of the PM metallic state may significantly be lowered by correlation effect beyond the HF approximation compared with the G-type AFM state.

The density of states for the G-type AFM and PM metallic states is shown in Fig. 16 for $\Delta=0.0$ eV and $\angle$Cu-O-Cu$=180°$. In the G-type AFM state, the character of the band gap is of the charge-transfer type. The density of

states is similar to that of the LDA+U calculation by Czyzyk and Sawatzky.[53] On the other hand, in the PM metallic state, both the Cu $3d$ and O $2p$ orbitals are strongly hybridized near the Fermi level. The density of state is similar to that of the LDA calculation.[53,55]

IV. CONCLUSION

The spin- and orbital-unrestricted HF calculations can explain the various magnetic and electronic properties of perovskite-type $3d$ transition-metal oxides, which are originated from the tenfold degeneracy or the spin and orbital degrees of freedom of the $3d$ orbitals. The HF calculations have revealed the interesting interplay between the orbital and spin ordering in the perovskite-type $3d$ transition-metal oxides with the partially filled t_{2g} or e_g orbital. It has also been found that the orbital-ordered states are strongly affected by the Jahn-Teller distortion and the $GdFeO_3$-type distortion. In the d^1 system, the FM solutions with the orbital ordering are stabilized both by the Jahn-Teller distortion and by the $GdFeO_3$-type distortion compared with the G-type AFM. In the d^2 system, the C-type and G-type AFM solutions with the orbital ordering are stabilized by the a-type and d-type Jahn-Teller distortions, respectively. In the high-spin d^4 compounds, while the FM state with the z^2-y^2, $3x^2$-r^2, $3y^2$-r^2, z^2-x^2-type orbital ordering is favored without the Jahn-Teller distortion, the Jahn-Teller distortion makes an A-type AFM state with the $3x^2$-r^2, $3y^2$-r^2, $3x^2$-r^2, $3y^2$-r^2-type orbital ordering lower in energy than the FM state. For the low-spin d^7 system, the observed magnetic structure is so complicated that the present HF calculation cannot give a clear description. However, in the HF calculation, the $GdFeO_3$-type distortion makes the magnitude of the band gap larger, which can explain the metallic versus insulating behavior of $RNiO_3$ as a function of the size of the R ion.

Although these HF results for the ground states are generally in good agreement with the experimental results, the magnitudes of the band gaps calculated by the HF approximation fail to explain the experimental results. We should include the fluctuation around the HF solution in order to explain the magnitude of the band gap and single-particle excitation spectrum.[56]

ACKNOWLEDGEMENTS

The authors wish to thank Dr. K. Tomimoto, Dr. H. Noma, Professor J. Akimitsu, Dr. N. Hamada, Dr. H. Sawada, Dr. I. V. Solevyev, Dr. V. I. Anisimov, and Professor D. I. Khomskii for useful discussions on orbital ordering in perovskite-type transition-metal oxides. We also appreciate Dr. H. Sawada, Dr. N. Hamada, and Dr. K. Terakura for showing us their numerical data of $YTiO_3$ prior to publication. Part of the calculations in this work were performed on a VAX computer in Meson Science Laboratory, University of Tokyo. The present work is supported by a Grant-in-Aid for Scientific Research from the Ministry of Education, Science and Culture and by the New Energy and Institute Technology Development Organization (NEDO).

[1] N. F. Mott, *Metal-Insulator Transitions* (Taylor & Francis, London, 1990).
[2] N. F. Mott, Proc. Phys. Soc. London, Sect. A **62**, 416 (1949).
[3] J. Hubbard, Proc. R. Soc. London, Ser. A **276**, 238 (1963); **277**, 237 (1964); **281**, 401 (1964).
[4] K. I. Kugel and D. I. Khomskii, Sov. Phys. Usp. **25**, 231 (1982); [Sov. Phys. JETP **37**, 725 (1973)].
[5] S. Inagaki and R. Kubo, Int. J. Magn. **4**, 139 (1973); S. Inagaki, J. Phys. Soc. Jpn. **39**, 596 (1975).
[6] M. Cyrot and C. Lyon-Caen, J. Phys. (Paris) **36**, 253 (1975); S. Wakoh, J. Phys. F. **7**, L15 (1977).
[7] C. Castellani, C. R. Natoli, and J. Ranninger, Phys. Rev. B **18**, 4945 (1975).
[8] J. Ashkenazi and M. Weger, Adv. Phys. **22**, 207 (1973).
[9] B. H. Brandow, Adv. Phys. **26**, 651 (1977).
[10] A. Fujimori and F. Minami, Phys. Rev. B **30**, 957 (1984).
[11] J. Zaanen, G. A. Sawatzky, and J. W. Allen, Phys. Rev. Lett. **55**, 418 (1985); S. Hüfner, Z. Phys. B **61**, 135 (1985).
[12] T. Mizokawa and A. Fujimori, Phys. Rev. B **51**, 12 880 (1995).
[13] M. D. Towler, R. Dovesi, and V. R. Saunders, Phys. Rev. B **52**, 10 150 (1995).
[14] V. I. Anisimov, J. Zaanen, and O. K. Andersen, Phys. Rev. B **44**, 943 (1991).
[15] A. I. Liechtenstein, V. I. Anisimov, and J. Zaanen, Phys. Rev. B **52**, R5467 (1995).
[16] J. Kanamori, Prog. Theor. Phys. **30**, 275 (1963).
[17] J. C. Slater and G. F. Koster, Phys. Rev. **94**, 1498 (1954).
[18] T. Mizokawa, A. Fujimori, T. Arima, Y. Tokura, N. Mori, and J. Akimitsu, Phys. Rev. B **52**, 13 865 (1995).
[19] A. E. Bocquet, T. Mizokawa, T. Saitoh, H. Namatame, and A. Fujimori, Phys. Rev. B **46**, 3771 (1992).
[20] T. Saitoh, A. E. Bocquet, T. Mizokawa, H. Namatame, A. Fujimori, M. Abbate, Y. Takeda, and M. Takano, Phys. Rev. B **51**, 13 942 (1995).
[21] T. Saitoh, A. E. Bocquet, T. Mizokawa, and A. Fujimori, Phys. Rev. B **52**, 7934 (1995); A. E. Bocquet, T. Mizokawa, K. Morikawa, A. Fujimori, S. R. Barman, K. Maiti, D. D. Sarma, Y. Tokura, and M. Onoda, *ibid.* **53**, 1161 (1996).
[22] J. van Elp, Ph.D. thesis, University of Groningen, 1991.
[23] T. Uozumi, K. Okada, and A. Kotani, J. Phys. Soc. Jpn. **62**, 2595 (1993).
[24] L. F. Mattheiss, Phys. Rev. B **5**, 290 (1972).
[25] J. B. Mann, Los Alamos Scientific Laboratory Report No. LASL-3690, 1967 (unpublished); F. M. F. de Groot, J. C. Fuggle, B. T. Tole, and G. A. Sawatzky, Phys. Rev. B **40**, 5715 (1990).
[26] A. Okazaki, J. Phys. Soc. Jpn. **26**, 870 (1969); M. T. Hutchings, E. J. Samuelsen, G. Shirane, and K. Hirakawa, Phys. Rev. B **188**, 919 (1969); N. Tsukuda and A. Okazaki, J. Phys. Soc. Jpn. **33**, 1088 (1972).
[27] E. O. Wollan and W. C. Koehler, Phys. Rev. **100**, 545 (1955).
[28] J. P. Goral and J. E. Greedan, J. Magn. Magn. Mater. **37**, 315 (1983).
[29] D. A. Crandles, T. Timusk, J. D. Garrett, and J. E. Greedan, Physica C **201**, 407 (1992).

[30] T. Arima, Y. Tokura, and J. B. Torrance, Phys. Rev. B **48**, 17 006 (1993).
[31] J. D. Garret and J. E. Greedan, Inorg. Chem. **20**, 1025 (1981).
[32] J. P. Goral, J. E. Greedan, and D. A. MacLean, J. Solid State Chem. **43**, 244 (1982); Y. Okimoto, T. Katsufuji, Y. Okada, T. Arima, and Y. Tokura, Phys. Rev. B **51**, 9581 (1995).
[33] J. Kanamori, J. Phys. Chem. Solids **10**, 87 (1959).
[34] D. A. MacLean, H.-N. Ng, and J. E. Greedan, J. Solid State Chem. **30**, 35 (1979).
[35] K. Tomimoto (private communication).
[36] W. A. Harrison, *Electronic Structure and the Properties of Solids* (Dover, New York, 1989).
[37] H. Sawada (private communication).
[38] Y. Fujishima, Y. Tokura, T. Arima, and S. Uchida, Phys. Rev. B **46**, 11 167 (1992); Y. Taguchi, T. Tokura, T. Arima, and F. Inaba, *ibid.* **48**, 511 (1993); Y. Tokura, Y. Taguchi, Y. Okada, Y. Fujishima, T. Arima, K. Kumagai, and Y. Iye, Phys. Rev. Lett. **70**, 2126 (1993); K. Kumagai, T. Suzuki, Y. Taguchi, Y. Okada, Y. Fujishima, and Y. Tokura, Phys. Rev. B **48**, 7636 (1993).
[39] V. G. Zubkov, G. V. Bazuev, V. A. Perelyaev, and G. P. Shveikin, Fiz. Tverd. Tela (Leningrad) **15**, 1610 (1973) [Sov. Phys. Solid State **15**, 107 (1973)]; N. Shirakawa and M. Ishikawa, Jpn. J. Appl. Phys. **30**, L775 (1991); P. Bordet, C. Chaillout, M. Marezio, Q. Huang, A. Santoro, S.-W. Cheong, H. Takagi, C. S. Oglesby, and B. Batlogg, J. Solid State Chem. **106**, 253 (1993); A. V. Mahajan, D. C. Jhonston, D. R. Orgeson, and F. Borsa, Phys. Rev. B **46**, 10 966 (1993).
[40] V. G. Zubkov, A. S. Borukhovich, G. V. Bazuev, I. I. Matveenko, and G. P. Shveikin, Zh. Éksp. Teor. Fiz. **66**, 1823 (1974) [Sov. Phys. JETP **39**, 896 (1974)]; H. Kawano, H. Yoshizawa, and Y. Ueda, J. Phys. Soc. Jpn. **63**, 2857 (1994).
[41] H. Sawada, N. Hamada, K. Terakura, and T. Asada, Phys. Rev. B **53**, 12 742 (1996).
[42] W. C. Koehler and E. O. Wollan, J. Phys. Chem. Solids **2**, 100 (1957).
[43] J. B. Goodenough, Phys. Rev. **100**, 564 (1955); G. Matsumoto, J. Phys. Soc. Jpn. **29**, 606 (1970); J. B. A. A. Elemans, B. van Laar, K. R. van der Veen, and B. O. Loopstra, J. Solid State Chem. **3**, 328 (1971).
[44] J. B. Goodenough, A. Wold, R. J. Aronott, and N. Menyuk, Phys. Rev. **124**, 373 (1961).
[45] G. H. Jonker and J. H. van Santen, Physica **16**, 337 (1950); Y. Tokura, A. Urushibara, Y. Moritomo, T. Arima, A. Asamitsu, G. Kido, and N. Furukawa, J. Phys. Soc. Jpn. **63**, 3931 (1994).
[46] A. Chainani, M. Mathew, and D. D. Sarma, Phys. Rev. B **47**, 15 397 (1993).
[47] G. H. Jonker and J. H. van Santen, Physica **19**, 120 (1953); P. M. Raccah and J. B. Goodenough, Phys. Rev. **155**, 932 (1967); G. Thoronton, B. C. Tofield, and D. E. Williams, Solid State Commun. **44**, 1213 (1982).
[48] T. Saitoh, Ph.D. thesis, University of Tokyo, 1996.
[49] M. A. Korotin, S. Yu. Ezhov, I. V. Solovyev, V. I. Anisimov, D. I. Khomskii, and G. A. Sawatzky (unpublished).
[50] A. Chainani, M. Mathew, and D. D. Sarma, Phys. Rev. B **46**, 9976 (1992).
[51] P. Lacorre, J. B. Torrance, J. Pannetier, A. I. Nazzal, P. W. Wang, and T. C. Huang, J. Solid State Chem. **91**, 225 (1991); J. B. Torrance, P. Lacorre, A. I. Nazzal, E. J. Ansaldo, and C. H. Niedermayer, Phys. Rev. B **45**, 8209 (1992); J. L. García-Muñoz, J. Rodríguez-Carvajal, P. Lacorre, and J. B. Torrance, *ibid.* **46**, 4414 (1992).
[52] J. L. García-Muñoz, J. Rodríguez-Carvajal, and P. Lacorre, Europhys. Lett. **20**, 241 (1992); J. L. García-Muñoz, J. Rodríguez-Carvajal, and P. Lacorre, Phys. Rev. B **50**, 978 (1994).
[53] M. T. Czyzyk and G. A. Sawatzky, Phys. Rev. B **49**, 14 211 (1994).
[54] G. Demazeau, C. Parent, M. Pouchard, and P. Hagenmuller, Mater. Res. Bull. **7**, 913 (1972); J. F. Bringley, B. A. Scott, S. J. La Placa, T. R. McGuire, F. Mehran, M. W. McElfresh, and D. E. Cox, Phys. Rev. B **47**, 15 269 (1993).
[55] N. Hamada, H. Sawada, and K. Terakura, in *Spectroscopy of Mott Insulators and Correlated Metals*, edited by A. Fujimori and Y. Tokura (Springer-Verlag, Berlin, 1995), p. 95.
[56] T. Mizokawa and A. Fujimori, Phys. Rev. B **53**, R4201 (1996).